PAPER

Check for updates

Construction of a crystalline 14-metal Zn–Nd rectangular nanocluster with a dual-emissive response towards metal ions†

Jieni Liu,[a] Xiaoping Yang, ✸*[a] Ting Zhu,[a] Bichen Yuan,[a] Hongfen Chen,[a] Dongliang Shi,[a] Desmond Schipper[b] and Richard A. Jones [b]

A crystalline 14-metal Zn–Nd cluster $[Zn_6Nd_8L_2(OAc)_{20}(O)_2(NO_3)_4(OC_2H_5)_4]$ (**1**) was constructed using a flexible Schiff base ligand with long-chain $(CH_2)_2O(CH_2)_2O(CH_2)_2$ backbone. **1** exhibits a nanoscale rectangular structure (10 × 14 × 18 Å). Besides the visible ligand-centered emission, **1** displays typical NIR luminescence of Nd^{3+}. Interestingly, **1** shows both a ligand-centered and lanthanide fluorescence response towards metal ions, especially to K^+ and Co^{2+} at the ppm level.

Introduction

A fluorescence response towards various analytes such as metal ions, acid radical anions and small molecules has recently gained considerable attention for its potential application in biology, medicine and environment.[1–3] For example, the fluorescence detection of potassium (K^+) is essential to biomedical diagnosis since potassium plays a central role in the human body. Recently, many crown ethers and cryptands have been used in the study of fluorescent K^+ sensors.[4–6] However, the results of the fluorescence intensity-based response may be easily affected by some factors such as the power of the light source and the concentration of the analyte. Recently, dual-emissive probes with two emission bands have been designed to make the response more accurate by the self-calibration of the fluorescence signals.[7–13] For example, some dual-emissive probes such as fluorescent organic compounds,[14,15] nanoparticles[16,17] and d-block metal complexes[18,19] have been used for this purpose in biologic imaging.

Lanthanide complexes are particularly attractive for the fluorescent response, due to their unique emission properties such as large Stokes shifts, high colour purity and long luminescence lifetimes. For example, near-infrared (NIR) luminescent lanthanide complexes with $Nd(III)$, $Yb(III)$ and $Er(III)$ ions have potential application in bioassays because biological tissues are transparent in this spectral range (900–1600 nm). So
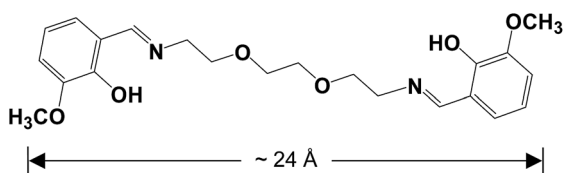
far, many visible luminescent lanthanide complexes with $Eu(III)$ and $Tb(III)$ ions have been used as sensors to detect analytes.[20–24] For example, a $Tb(III)$ complex with 18-crown-6 ligand has been used for the time-gated luminescence detection of K^+ ion.[25] However, there are very few reports on the dual-emissive probes based on lanthanide complexes. Recently, Chi *et al.* first reported the detection of water in organic solvents using a dual-emissive $Eu(III)$-based metal–organic framework (MOF) encapsulating carbon-based dots (CDs), where both red light emission from Eu^{3+} ions and blue light emission from CDs show response to the water.[26] For the NIR luminescent lanthanide complexes, besides the lanthanide luminescence around 900–1600 nm, they can exhibit ligand-centered emission in the visible region. Dual-emissive probes based on emissions from both lanthanide ion and organic ligand may have some advantages in the detection of target objects, due to the difference between the emissions in their lifetimes, wavelengths and band shapes.

Compared with the visible luminescence of lanthanide ions such as $Eu(III)$ and $Tb(III)$, the NIR lanthanide luminescence is much far apart from the ligand-centered emission (usually at near 500 nm). Thus, the purpose of our research is to design dual-emissive lanthanide-based probes with both visible ligand-centered emission and NIR lanthanide luminescence. It is known that, some metal chromophores with d-block transition-metal ions such as $Zn(II)$, $Ru(II)$, $Pt(II)$ and $Cd(II)$ may not only show strong visible emission, but also can act as sensitizers for the NIR lanthanide luminescence ("antenna effect"). Our current research has focused on the luminescent response of d–4f nanoclusters towards various analytes.[27,28] Here, one crystalline 14-metal Zn–Nd cluster $[Zn_6Nd_8L_2(OAc)_{20}(O)_2(NO_3)_4(OC_2H_5)_4]$ (**1**) was prepared using a long-chain Schiff base ligand N,N'-bis(3-methoxysalicylidene)(1,2-bis(ethoxy)ethane)-1,6-diamine (H_2L, Scheme 1). The length of H_2L is about 24 Å, which is much longer than most of other reported flexible Schiff

aZhejiang Key Laboratory of Carbon Materials, College of Chemistry and Materials Engineering, Wenzhou University, Wenzhou 325035, China. E-mail: xpyang@wzu.edu.cn

bDepartment of Chemistry and Biochemistry, The University of Texas at Austin, 1 University Station A5300, Austin, Texas, 78712, USA
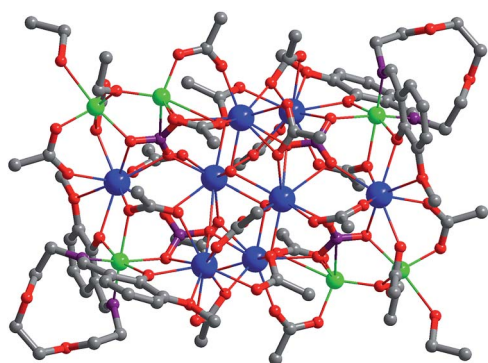
Scheme 1 Long-chain Schiff base ligand H_2L.

base ligands with no more than 5 methylene (CH_2) units in the backbones. **1** exhibits a nanoscale rectangular structure (10 × 14 × 18 Å). In the rectangular structure of **1**, there are total 66 electronegative O atoms from Schiff base ligands and anions, which may help to form intermolecular interaction with added cations through electrostatic force. Interestingly, **1** shows both lanthanide and ligand-centered fluorescent response to metal ions, especially to K^+ and Co^{2+} ions.

Results and discussion

Synthesis and crystal structure of 1

The Schiff-base ligand H_2L was prepared from the reaction of 2-[2-(2-amion-ethoxy)-ethoxy]-ethylanine and 2-hydroxy-3-methoxy-benzaldehyde, according to well established procedures.[29] The reaction of H_2L with $Zn(OAc)_2 \cdot 2H_2O$ and $Nd(NO_3)_3 \cdot 6H_2O$ gave a yellow solution, and **1** was obtained by the diffusion of diethyl ether into the solution as pale yellow crystalline solid. As shown in Fig. 1, the crystal structure of **1** is centrosymmetric. Six Zn^{2+} and eight Nd^{3+} ions are linked together by two Schiff base ligands, twenty OAc^-, two O^{2-} and four NO_3^- anions. The $Zn(II)\cdots Nd(III)$ distances are from 3.706 Å to 3.897 Å. The OAc^-, O^{2-} and NO_3^- anions exhibit μ_2, μ_3 and μ_5 coordination modes with the metal ions, respectively. All Nd^{3+} ions are surrounded by O atoms from the Schiff base ligands and anions. Six Nd^{3+} ions are nine-coordinated with single cap square antiprism geometry, while other two are ten-coordinated with pseudo-bicapped square-antiprismatic geometry. In **1**, Zn^{2+} ions show tetrahedral, triangular bipyramidal and octahedron geometries. For the Schiff base ligands in **1**, their N atoms coordinate to two six-coordinated Zn^{2+} ions, and the phenoxide and methoxy O atoms bind to four Nd^{3+} ion, while the backbone O atoms do not coordinate to the metal ions. The

Zn–N, Zn–O, Nd–N and Nd–O bond lengths are 2.082 Å–2.099 Å, 1.906 Å–2.444 Å, 2.916 Å–2.970 Å and 2.395 Å–2.666 Å, respectively.
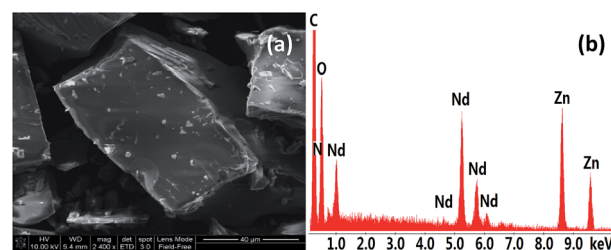
The panoramic scanning electron microscopy (SEM) image and energy dispersive X-ray spectroscopy (EDX) spectrum of **1** are shown in Fig. 2. The element integration data of the EDX spectrum show that molar ratio of Zn/Nd is 3.2 : 4, which is close to the ration (3 : 4) calculated by the crystal structure. The powder XRD pattern of **1** is similar to the simulated pattern generated from the single crystal X-ray diffraction data (Fig. S2†). Thermogravimetric analysis exhibits that when **1** is heated at 100 °C, it loses about 8% of the weight (Fig. S3†). This is due to the escaping of the uncoordinated solvent molecules. **1** starts to discompose when the temperature is 155 °C (Experimental). Molar conductivity study confirms that **1** is neutral in CH_3CN, in agreement with the crystal structure.

Photophysical properties

The luminescence properties of **1** were studied in CH_3CN and the solid state. The UV-vis absorption spectra show that the absorption bands of **1** are red-shifted compared with those of the free H_2L (Fig. 3). Upon the excitation in ligand absorption band at 355 nm, **1** exhibits typical NIR luminescence of Nd^{3+} ($^4F_{3/2} \rightarrow {}^4I_{j/2}$ transitions, j = 9, 11 and 13), and the most intense line is at 1061 nm ($^4F_{3/2} \rightarrow {}^4I_{11/2}$, Fig. 4). Besides the lanthanide luminescence, the ligand-centered emission of **1** is found at 494 nm. **1** shows similar emission spectra in CH_3CN and the solid state. The NIR emission lifetime (τ) of **1** in CH_3CN is 5.5 μs (Fig. S4†). Thus, the intrinsic quantum yield (Φ_{Ln}) of Nd^{3+} in **1** is calculated to be 2.2% ($\Phi_{Ln} = \tau/\tau_0$, τ_0 = 250 μs, the natural lifetime of Nd^{3+}).[30] The overall NIR emission quantum yield (Φ_{em}) of **1** is 0.7%. The energy transfer efficiency ($\eta_{sens} = \Phi_{em}/\Phi_{Ln}$) from ligand to lanthanide ion in **1** is estimated to be 31.8%.[31]

Luminescent sensing towards metal ions

The NIR lanthanide luminescent and visible ligand-centered fluorescent response behaviour of **1** to metal ions Cr^{3+}, Mn^{2+}, Fe^{3+}, Co^{2+}, Ni^{2+}, Cu^{2+}, Zn^{2+}, Cd^{2+}, Ag^+, Mg^{2+}, Sr^{2+}, Al^{3+}, Li^+, Na^+ and K^+ (metal acetates) have been investigated in DMF. Interestingly, the addition of metal ions results in different intensity changes of the emissions. For example, the addition of all metal ions decreases the lanthanide luminescence of **1**. The addition of metal ions K^+, Li^+, Na^+, Ag^+, Mg^{2+}, Al^{3+}, Cr^{3+} and Sr^{2+} increases the ligand-centered emission, but the addition of

Fig. 1 The crystal structure of **1** (Nd^{3+}: blue; Zn^{2+}: green).

Fig. 2 Scanning electron microscopy image (a) and energy dispersive X-ray spectroscopy spectrum (b) of **1**.

Fig. 3 UV-visible absorption spectra of the free Schiff base ligand H_2L and **1** in CH_3CN.

Fig. 6 Ligand-centered fluorescent response of **1** (60 μM) to the addition of K(OAc) in DMF (λ_{ex} = 355 nm).
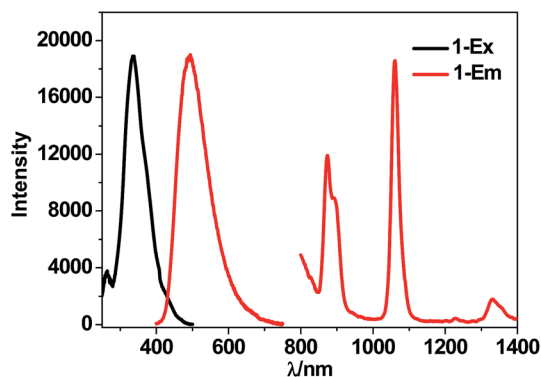

Fig. 4 Excitation and emission spectra of **1** in CH_3CN at room temperature (λ_{ex} = 355 nm).

others decreases the emission (Fig. 5, 6 and S5, S6†). It is found that the addition of K^+ and Co^{2+} ions causes a more rapid decrease of the lanthanide luminescence intensity than the addition of other metal ions. For example, the emission intensities at 1061 nm of **1** are decreased about 50% when the concentrations of added K^+ and Co^{2+} solutions are 255 μM and 109 μM, respectively (Fig. 5 and S5†). Compared with other metal ions, the addition of K^+ (or Co^{2+}) ion also leads to a more
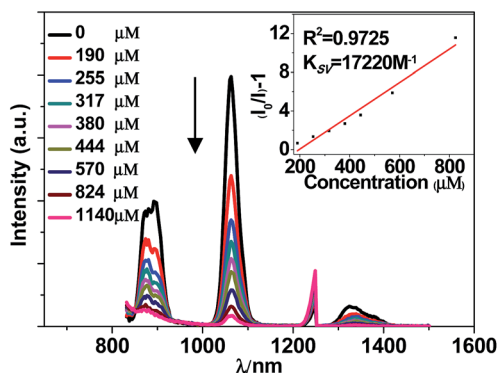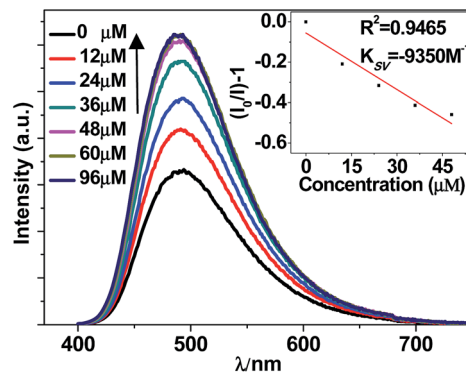
rapid enhancement (or decrease) of the ligand-centered emission. For example, with the addition of 60 μM K^+ (or 44 μM Co^{2+}) ion, the ligand-centered emission intensity at 494 nm is increased by one time (or decreased by a half) (Fig. 6 and S6†). These results indicate that, compared with other metal ions, **1** shows high sensitivity to K^+ and Co^{2+} ions through both lanthanide and ligand-centered fluorescent response.

The intensity changes for both lanthanide and ligand-centered emissions of **1** and the concentrations of the added metal ions show a linear relationship. Thus, the emission quenching and enhancement efficiencies (K_{SV}) of **1** can be calculated by using $K_{SV} = (I_0/I - 1)/[A]$ (Stern–Volmer equation).[32] Here, I_0 and I are the emission intensities of **1** at 1065 (or 494) nm before and after the addition of metal ion, respectively [A] is the concentration of added metal ion. The K_{SV} values for the lanthanide and ligand-centered emission sensing of **1** towards metal ions are shown in Fig. 7 and 8. For the lanthanide luminescence, the K_{SV} values of **1** to K^+ and Co^{2+} ions are 17.2 × 10^3 M^{-1} and 12.7 × 10^3 M^{-1}, respectively. While, for the ligand-centered emission, the K_{SV} values of **1** to K^+ and Co^{2+} ions are −9.4 × 10^3 M^{-1} and 58.7 × 10^3 M^{-1}, respectively. All these K_{SV} values to K^+ and Co^{2+} ions are greater than corresponding values to other metal ions. The limits of detection (LOD) of **1** to metal ions can be estimated by the signal-to-noise ratio (S/N = 3), using LOD = $3\sigma/K_{SV}$,[33] where σ is the standard deviation. For

Fig. 5 Lanthanide luminescent response of **1** (60 μM) to the addition of K(OAc) in DMF (λ_{ex} = 355 nm).
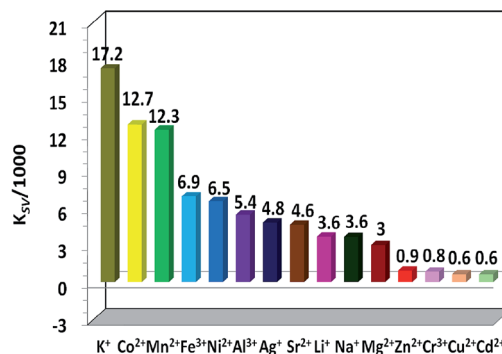

Fig. 7 Lanthanide luminescence quenching efficiencies (K_{SV}) of **1** towards metal cations.
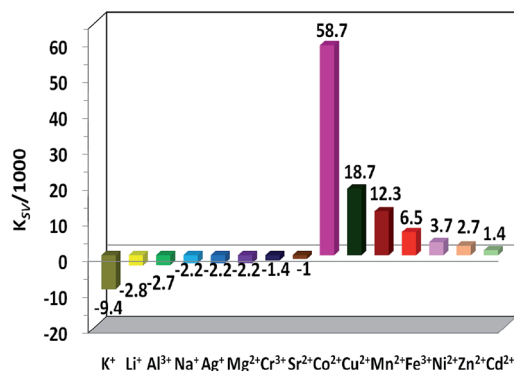
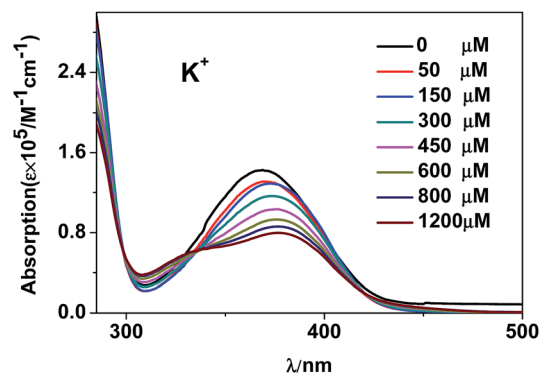**Fig. 8** Ligand-centered emission enhancement efficiencies (K_{SV}) of **1** towards metal cations.

Fig. 9 UV-vis spectra of **1** (60 μM) with the addition of K^+ ion.

the lanthanide (or ligand-centered) emission sensing, the LOD data of **1** to K^+ and Co^{2+} ions are calculated to be 3.67 μM (or 1.87 μM) and 4.96 μM (or 2.97 μM), respectively. These results indicate that **1** show both lanthanide and ligand-centered fluorescent response to these metal ions at the ppm level.

The underlying principles of fluorescence response of sensors towards metal ions are so-called chelation enhancement of the quenching emission (CHEQ) and chelation-enhanced fluorescence chelation-enhanced fluorescence (CHEF) effects.[34] These effects are determined by a series of transduction mechanisms based on energy transfer and charge transfer processes. The added metal ions may affect the energy transfer and charge transfer processes in different ways, resulting in various CHEQ and CHEF effects to the emissions of **1**. For example, d-block metal ions Co^{2+}, Mn^{2+}, Fe^{3+}, Ni^{2+}, Cr^{3+} and Cu^{2+} ions have d–d transitions due to their unfilled d electronic configurations. Thus, these metal ions may consume the excitation energy of lanthanide ions through f → d energy transfers,[35] resulting in the decrease of lanthanide luminescence. In addition, the added metal ions may affect the ligand-to-metal energy transfer process because of their perturbation to the electronic structure and excited state of the ligand, leading to various intensity changes of the lanthanide luminescence and ligand-centered emission of **1**. As shown in Fig. 8, differing from the addition of other 3d metal ions Co^{2+}, Cu^{2+}, Mn^{2+}, Fe^{3+}, Ni^{2+} and Zn^{2+}, which decreases the ligand-centered emission of **1**, the addition of Cd^{3+} ion increases the ligand-centered emission. This may be explained by the presence of the ligand-to-metal charge transfer (LMCT) transition resulted by the additional of metal ion.[36,37]

It is found that, the intensity changes of visible and NIR emissions of **1** are not proportional to the radii of added metal ions (Fig. S7†). In fact, the interaction between the added metal ions and **1** plays a key role in both lanthanide and ligand-centered fluorescent response. For example, K^+ ion has been reported to be easy to form some intermolecular interaction such as cation–π interaction with macrocyclic compounds and framework complexes due to its suitable ionic size.[25,38–41] The interaction between the added metal ions and **1** was investigated by UV-vis titration measurement (Fig. S8†).[42] As shown in

Fig. 9, the addition of K^+ ion results in a red-shift of the absorption bands of **1**, which confirms the formation of intermolecular interaction between K^+ ion and the complex.

Experimental

Synthesis of the crystalline cluster $[Zn_6Nd_8L_2(OAc)_{20}(O)_2(NO_3)_4(OC_2H_5)_4]$ (1)

$Zn(OAc)_2 \cdot 2H_2O$ (0.30 mmol, 0.0666 g), $Nd(NO_3)_3 \cdot 6H_2O$ (0.40 mmol, 0.1800 g) and H_2L (0.10 mmol, 0.0417 g) were dissolved in 10 mL EtOH, 2 mL MeOH and 2 mL DMF at room temperature, and a solution of triethylamine in EtOH (0.01 mol L^{-1}, 2 mL) was then added. The resulting solution was heated under reflux for 30 min. It was filtered at room temperature. The yellow crystalline product of **1** was obtained by the slow diffusion of diethyl ether into the filtrate at room temperature after three weeks. The product was collected and dried in the oven at 120 °C for two hours. Yield: 0.0672 g (32%). Mp > 155 °C (dec.). Elemental analysis: found: C, 28.85; H, 3.71; N, 2.63%. Calc. for $C_{100}H_{152}N_8O_{72}Zn_6Nd_8$: C, 28.84; H, 3.68; N, 2.69%. IR (cm^{-1}): 1624 (s), 1552 (s), 1450 (m), 1408 (m), 1295 (m), 1212 (s), 1076 (m), 962 (m), 852 (w), 784 (m), 741 (s), 673 (m).

Crystallography

X-ray data were collected for **1** on a Smart APEX CCD diffractometer at 190 K in the θ–2θ mode with monochromated Mo Kα radiation. The direct method (SHELX 97 program) was used to solve the structures. Non-hydrogen atoms were refined anisotropically, while hydrogen atoms were included but not refined. The selected bond lengths and angles for the structure of **1** are listed in Table S1.†

1: $C_{100}H_{152}N_8O_{72}Zn_6Nd_8$, triclinic, space group $P\bar{1}$, $a = 14.1791(12)$, $b = 15.7934(13)$, $c = 18.0220(15)$ Å, $\alpha = 108.2630(10)°$, $\beta = 96.2280(10)°$, $\gamma = 108.4170(10)°$, $V = 3538.5(5)$ Å^3, $Z = 1$, $D_c = 1.954$ g cm^{-3}, μ(Mo Kα) = 3.971 mm^{-1}, $F(000) = 2044$, $T = 190$ K. $R_1 = 0.0314$, $wR_2 = 0.1021$, GOF = 1.129.

Conclusions

In conclusion, one crystalline 14-metal Zn–Nd complex **1** was constructed using a flexible Schiff base ligand with long-chain $(CH_2)_2O(CH_2)_2O(CH_2)_2$ backbone. **1** has nanoscale rectangular molecular size ($10 \times 14 \times 18$ Å). Upon the excitation of absorption bands, **1** exhibits visible ligand-centered and NIR lanthanide emissions. The addition of K^+, Li^+, Na^+, Ag^+, Mg^{2+}, Al^{3+} and Cr^{3+} ions increases the intensity of ligand-centered emission of **1**, however, the addition of Co^{2+}, Cu^{2+}, Mn^{2+}, Ni^{2+}, Zn^{2+} and Cd^{2+} ions decreases the intensity. While, the addition of metal ions decreases the lanthanide luminescence of **1**. Compared with other metal ions, **1** shows high sensitivity to K^+ and Co^{2+} ions at the ppm level through both lanthanide and ligand-centered fluorescent response. Further studies focused on the dual-emissive response of lanthanide-based clusters to other analytes are in progress.

Conflicts of interest

There are no conflicts to declare.

Acknowledgements

Notes and references

1 X. Qi, Y. Jin, N. Li, Z. Wang, K. Wang and Q. Zhang, *Chem. Commun.*, 2017, **53**, 10318–10321.
2 X. Sun, Y. Wang and Y. lei, *Chem. Soc. Rev.*, 2015, **44**, 8019–8061.
3 J. Jankolovits, C. M. Andolina, J. W. Kampf, K. N. Raymond and V. L. Pecoraro, *Angew. Chem., Int. Ed.*, 2011, **50**, 9660–9664.
4 H. Kager, W. J. Wadman and G. G. Somjen, *J. Neurophysiol.*, 2000, **84**, 495–512.
5 V. Petrilli, S. Papin, C. Dostert, A. Mayor, F. Martinon and J. Tschopp, *Cell Death Differ.*, 2007, **14**, 1583–1589.
6 J. K. Tusa and H. He, *J. Mater. Chem.*, 2005, **15**, 2640–2647.
7 Y. Bretonnière, M. J. Cann, D. Parker and R. Slater, *Chem. Commun.*, 2002, 1930–1931.
8 D. Parker and J. Yu, *Chem. Commun.*, 2005, 3141–3143.
9 M. S. Tremblay, M. Halim and D. Sames, *J. Am. Chem. Soc.*, 2007, **129**, 7570–7577.
10 R. Pal and D. Parker, *Org. Biomol. Chem.*, 2008, **6**, 1020–1033.
11 S. E. Plush and T. Gunnlaugsson, *Dalton Trans.*, 2008, 3801–3804.
12 Z. Li, Z. Hou, D. Ha and H. Li, *Chem.–Asian J.*, 2015, **10**, 2720–2724.
13 Y. Okayasu, H. Kabemuchi and J. Yuasa, *Dalton Trans.*, 2018, **47**, 6779–6786.
14 S. Takahashi, W. Piao, Y. Matsumura, T. Komatsu, T. Ueno, T. Terai, T. Kamachi, M. Kohno, T. Nagano and K. Hanaoka, *J. Am. Chem. Soc.*, 2012, **134**, 19588–19591.
15 C. Huang, T. Jia, M. Tang, Q. Yin, W. Zhu, C. Zhang, Y. Yang, N. Jia, Y. Xu and X. Qian, *J. Am. Chem. Soc.*, 2014, **136**, 14237–14244.
16 K. Y. Zhang, J. Zhang, Y. Liu, S. Liu, P. Zhang, Q. Zhao, Y. Tang and W. Huang, *Chem. Sci.*, 2015, **6**, 301–307.
17 H. Ma, B. Song, Y. Wang, D. Cong, Y. Jiang and J. Yuan, *Chem. Sci.*, 2017, **8**, 150–159.
18 K. Y. Zhang, H. Liu, M. Tang, A. W. Choi, N. Zhu, X. Wei, K. Lau and K. K. Lo, *Inorg. Chem.*, 2015, **54**, 6582–6593.
19 T. Yoshihara, Y. Yamaguchi, M. Hosaka, T. Takeuchi and S. Tobita, *Angew. Chem., Int. Ed.*, 2012, **51**, 4148–4151.
20 B. Chen, L. Wang, Y. Xiao, F. R. Fronczek, M. Xue, Y. Cui and G. Qian, *Angew. Chem., Int. Ed.*, 2009, **48**, 500–503.
21 P. F. Shi, H. C. Hu, Z. Y. Zhang, G. Xiong and B. Zhao, *Chem. Commun.*, 2015, **51**, 3985–3988.
22 Y. Qiu, H. Deng, J. Mou, S. Yang, M. Zeller, S. R. Batten, H. Wu and J. Li, *Chem. Commun.*, 2009, 5415–5417.
23 G. L. Liu, Y. J. Qin, L. Jing, G. Y. Wei and H. Li, *Chem. Commun.*, 2013, **49**, 1699–1701.
24 Z. Guo, H. Xu, S. Su, J. Cai, S. Dang, S. Xiang, G. Qian, H. Zhang, M. O'Keeffe and B. Chen, *Chem. Commun.*, 2011, **47**, 5551–5553.
25 A. Thibon and V. C. Pierre, *J. Am. Chem. Soc.*, 2009, **131**, 434–435.
26 Y. Dong, J. Cai, Q. Fang, X. You and Y. Chi, *Anal. Chem.*, 2016, **88**, 1748–1752.
27 C. Wang, X. Yang, S. Wang, T. Zhu, L. Bo, L. Zhang, H. Chen, D. Jiang, X. Dong and S. Huang, *J. Mater. Chem. C*, 2018, **6**, 865–874.
28 D. Jiang, X. Yang, X. Zheng, L. Bo, T. Zhu, H. Chen, L. Zhang and S. Huang, *J. Mater. Chem. C*, 2018, **6**, 8513–8521.
29 F. Lam, J.-X. Xu and K.-S. Chan, *J. Org. Chem.*, 1996, **61**, 8414–8418.
30 S. I. Klink, L. Grave, D. N. Reinhoudt, F. C. J. M. v. Veggel, M. H. V. Werts, F. A. J. Geurts and J. W. Hofstraat, *J. Phys. Chem. A*, 2000, **104**, 5457–5468.
31 J. C. G. Bünzli and C. Piguet, *Chem. Soc. Rev.*, 2005, **34**, 1048–1077.
32 Y. Xiao, Y. Cui, Q. Zheng, S. Xiang, G. Qian and B. Chen, *Chem. Commun.*, 2010, **46**, 5503–5505.
33 X. Qi, Y. Jin, N. Li, Z. Wang, K. Wang and Q. Zhang, *Chem. Commun.*, 2017, **53**, 10318–10321.
34 M. A. Treto-Suárez, Y. Hidalgo-Rosa, E. Schott, X. Zarate and D. Páez-Hernández, *J. Phys. Chem. A*, 2019, **123**, 6970–6977.
35 X. Wen, Y. Zhao, L. Wang, M. Zhang and D. Gao, *J. Rare Earths*, 2007, **25**, 679–683.
36 Z. Hu, B. J. Deibert and J. Li, *Chem. Soc. Rev.*, 2014, **43**, 5815–5840.
37 A. Bourdolle, M. Allali, J. C. Mulatier, B. L. Guennic, J. M. Zwier, P. L. Baldeck, J. C. G. Bünzli, C. Andraud, L. Lamarque and O. Maury, *Inorg. Chem.*, 2011, **50**, 4987–4999.
38 Z. Han, Z. Xiao, M. Hao, D. Yuan, L. Liu, N. Wei, H. Yao and M. Zhou, *Cryst. Growth Des.*, 2015, **15**, 531–533.

39 X. Zhou, F. Su, Y. Tian, C. Youngbull, R. H. Johnson and D. R. Meldrum, *J. Am. Chem. Soc.*, 2011, **133**, 18530–18533.

40 B. J. Müller, S. M. Borisov and I. Klimant, *Adv. Funct. Mater.*, 2016, **26**, 7697–7707.

41 B. Sui, X. Yue, B. Kim and K. D. Belfield, *ACS Appl. Mater. Interfaces*, 2015, **7**, 17565–17568.

42 C.-L. Liu, L.-P. Zhou, D. Tripathy and Q.-F. Sun, *Chem. Commun.*, 2017, **53**, 2459–2462.